Biochemical and Biophysical Research Communications 448 (2014) 163–168

Contents lists available at ScienceDirect

Biochemical and Biophysical Research Communications

journal homepage: www.elsevier.com/locate/ybbrc

Crystal structure and biochemical properties of the (*S*)-3-hydroxybutyryl-CoA dehydrogenase PaaH1 from *Ralstonia eutropha*

Jieun Kim [a,1], Jeong Ho Chang [b,1], Kyung-Jin Kim [a,*]

[a] School of Life Sciences, KNU Creative BioResearch Group (BK21 Plus Program), Kyungpook National University, Daehak-ro 80, Buk-ku, Daegu 702-701, Republic of Korea
[b] Department of Biology, Teachers College, Kyungpook National University, Daehak-ro 80, Buk-ku, Daegu 702-701, Republic of Korea

ARTICLE INFO

Article history:
Received 3 April 2014
Available online 29 April 2014

Keywords:
(*S*)-3-Hydroxybutyryl-CoA dehydrogenase
Ralstonia eutropha
n-Butanol
Crystal structure

ABSTRACT

3-Hydroxybutyryl-CoA dehydrogenase is an enzyme involved in the synthesis of the biofuel *n*-butanol by converting acetoacetyl-CoA to 3-hydroxybutyryl-CoA. To investigate the molecular mechanism of *n*-butanol biosynthesis, we determined crystal structures of the *Ralstonia eutropha*-derived 3-hydroxybutyryl-CoA dehydrogenase (*Re*PaaH1) in complex with either its cofactor NAD^+ or its substrate acetoacetyl-CoA. While the biologically active structure is dimeric, the monomer of *Re*PaaH1 comprises two separated domains with an N-terminal Rossmann fold and a C-terminal helical bundle for dimerization. In this study, we show that the cofactor-binding site is located on the Rossmann fold and is surrounded by five loops and one helix. The binding mode of the acetoacetyl-CoA substrate was found to be that the adenosine diphosphate moiety is not highly stabilized compared with the remainder of the molecule. Residues involved in catalysis and substrate binding were further confirmed by site-directed mutagenesis experiments, and kinetic properties of *Re*PaaH1were examined as well. Our findings contribute to the understanding of 3-hydroxybutyryl-CoA dehydrogenase catalysis, and will be useful in enhancing the efficiency of *n*-butanol biosynthesis by structure based protein engineering.

1. Introduction

Due to issues such as limited fossil fuel availability, greenhouse gas emissions, and the requirement for increased energy security or diversity, there is increased public and scientific interest in energy alternatives such as biofuels. A wide range of biofuels can be derived from plant or microbial biomass [1]. The two major biofuels in use today are ethanol and butanol, which can be combined with gasoline for use in conventional engines [2,3]. However, ethanol has a low energy efficiency compared to gasoline and high vaporizability [4]. Alternatively, *n*-butanol produced by microbial fermentation has characteristics that are closer to those of motor-vehicle fuels and could serve as a better replacement [5]. The anaerobic bacterium *Clostridium acetobutylicum* can efficiently produce *n*-butanol through a carbohydrate catabolic pathway [6,7]. In comparison with bio-ethanol, the advantage of the biosynthesized *n*-butanol is that it has a high energy content, low corrosion, increased solubility, and easier to blend with gasoline [8–10].

Even if *n*-butanol is considered a potential next generation biofuel source, its biosynthetic efficiency must be improved, and there have been multiple attempts to do so [11]. For example, many engineering efforts ranging from genetic modifications to microbial culture optimization, have aimed to increase *n*-butanol production during ABE fermentation. However, the *n*-butanol synthetic titers do not exceed 1 g/L in heterologous host cells that express clostridial *n*-butanol biosynthetic machinery [7–10]. Very recently, alternative methods to enhance the *n*-butanol yield have been reported; these involve the use of metabolically engineered hosts such as *Escherichia coli*, *Pseudomonas putida*, and *Bacillus subtilis* in the *n*-butanol biosynthetic pathway to improve biofuel production from small organic molecules [12–14].

A next step to produce large amount of *n*-butanol is the engineering of non-solventogenic microbes [15]. It has been shown that the *n*-butanol inhibits *E. coli* growth for example, the growth is almost ceased at approximately *n*-butanol concentrations of 1% [16], therefore, the toxicity effects of *n*-butanol in bacterial cells should be moderated [17]. Another issue is that the additive pathways for *n*-butanol synthesis disrupt the balance of energy carriers such as $NADH/NAD^+$, which results in a decrease in *n*-butanol

* Corresponding author. Address: Structural and Molecular Biology Laboratory, School of Life Sciences, Kyungpook National University, Daehak-ro 80, Buk-ku, Daegu 702-701, Republic of Korea. Fax: +82 53 955 5522.
E-mail address: kkim@knu.ac.kr (K.-J. Kim).
[1] These authors contributed equally to this work.

http://dx.doi.org/10.1016/j.bbrc.2014.04.101
0006-291X/

production [18]. These multiple issues have necessitated an optimization of the heterologous metabolic pathways to maximize the *n*-butanol biosynthetic yield by the use of engineered non-solventogenic microbes [18,19].

In contrast to *C. acetobutylicum*, which is a representative *n*-butanol producing host, *Ralstonia eutropha* has a broader spectrum and is used in the production of polymers such as polyhydroxybutyrate (PHB). It has been reported that the 3-hydroxybutyryl-CoA dehydrogenase PaaH1 is involved in *n*-butanol biosynthesis [20], and *R. eutropha*-derived PaaH1 is proposed as a homolog of *Clostridium butyricum* 3-hydroxybutyryl-CoA dehydrogenase (*Cb*HBD) that is involved in the second step of *n*-butanol biosynthesis [21]. Here, we report the first crystal structure of *R. eutropha* 3-hydroxybutyryl-CoA dehydrogenase (*Re*PaaH1), an enzyme that catalyzes the second step of *n*-butanol biosynthesis and converts acetoacetyl-CoA to 3-hydroxybutyryl-CoA. Kinetic properties and mutagenesis experiments were also reported.

2. Materials and methods

2.1. Preparation of RePaaH1

Cloning, expression, purification, and crystallization of *Re*PaaH1 will be described elsewhere. Briefly, the *Re*PaaH1 coding gene (Met1-Lys284, M.W. 32 kDa) was amplified by polymerase chain reaction (PCR) using *R. eutropha* chromosomal DNA as a template. The PCR product was then subcloned into pET30a (Invitrogen) with 6-histag at the C-terminus. The expression construct was transformed into an *E. coli* B834 strain, which was grown in 1 L of LB medium containing kanamycin (50 mg/ml) at 37 °C. After induction via the addition of 1.0 mM IPTG, the culture medium was further maintained for 20 h at 18 °C. The culture was harvested by centrifugation at 5000 × *g* at 4 °C. The cell pellet was resuspended in buffer A (40 mM Tris–HCl at pH 8.0 and 5 mM β-mercaptoethanol) and then disrupted by ultrasonication. The cell debris was removed by centrifugation at 11,000 × *g* for 1 h, and lysate was bound to Ni–NTA agarose (QIAGEN). After washing with buffer A containing 20 mM imidazole, the bound proteins were eluted with 300 mM imidazole in buffer A. A trace amount of contamination was removed by applying HiLoad 26/60 Superdex 200 prep grade (GE Healthcare) size exclusion chromatography. The purified protein showed ~95% purity on SDS–PAGE, was concentrated to 50 mg/ml in 40 mM Tris–HCl, pH 8.0, 1 mM dithiothreitol.

2.2. Crystallization, data collection, and structure determination of RePaaH1

Suitable crystals for diffraction experiments were obtained at 22 °C within 7 days from the precipitant of 2 M $(NH_4)_2SO_4$, 0.1 M Cacodylate pH 6.5 and 0.2 M Sodium Chloride. The crystals were transferred to cryoprotectant solution containing 2 M $(NH_4)_2SO_4$, 0.1 M Cacodylate pH 6.5, 0.2 M Sodium Chloride and 30% glycerol, fished out with a loop larger than the crystals and flash-frozen by immersion in liquid nitrogen at −173 °C. The data were collected to a resolution of 2.6 Å at 7A beamline of the Pohang Accelerator Laboratory (PAL, Pohang, Korea) using a Quantum 270 CCD detector (ADSC, USA). The data were then indexed, integrated, and scaled using the HKL2000 suite [22]. The data statistics are summarized in Table 1. Crystals of an apo-form belonged to space group $p3_221$, with unit cell parameters of $a = b = 135.43$ Å, $c = 97.17$ Å, $\alpha = \beta = 90$ and $\gamma = 120$. Assuming 3 molecules of *Re*PaaH1 per asymmetric unit, the crystal volume per unit of protein mass was 2.68 Å^3 Da^{-1} [23], which corresponds to a solvent content of approximately 54.12%. *Re*PaaH1 crystals in complex with NAD^+ and with acetoacetyl-CoA were crystallized with the same crystallization condition supplemented with 20 mM each of NAD^+ and acetoacetyl-CoA. Crystals in complex with NAD^+ belonged to space group *C*2, with unit cell parameters of $a = 235.08$ Å, $b = 135.59$ Å, $c = 97.45$ Å, $\alpha = \gamma = 90$ and $\beta = 90.1$. Assuming 9 molecules of *Re*PaaH1 per asymmetric unit, the crystal volume per unit of protein mass was 2.70 Å^3 Da^{-1} [23], which corresponds to a solvent content of approximately 54.41%. Crystals in complex with acetoacetyl-CoA belonged to the same space with *Re*PaaH1-NAD^+ complex crystals with similar unit cell parameters. SeMet-substituted apo-form crystals were obtained using the same crystallization condition as used for the native protein crystal. Single-wavelength anomalous dispersion (SAD) data were collected from an SeMet protein crystal on beamline 7A at PAL to a wavelength of 0.97855 Å. 36 Se atoms out of the expected 39 in the asymmetric unit were identified at 2.42 Å resolution using SOLVE [24]. The electron density was improved by density modification using RESOLVE [25], resulting in 54% of the cloned residues being automatically built.

Further model building was performed manually using the program WinCoot [26] and the refinement was performed with REFMAC5 [27]. The structures of *Re*PaaH1 in complex with NAD^+ and with acetoacetyl-CoA were solved by molecular replacement using the crystal structure of the apo-form of *Re*PaaH1. The refined model of apo-form of *C Re*PaaH1 and those in complex with NAD^+ and with acetoacetyl-CoA were deposited in the Protein Data Bank (pdb code 4PZC for apo-form of *Re*PaaH1, and 4PZD and 4PZE for NAD^+ and acetoacetyl-CoA bound forms of *Re*PaaH1, respectively).

2.3. 3-Hydroxybutyryl-CoA dehydrogenase activity measurement

All assays were performed with reaction mixture of 1 ml total volume. The reaction mixture contained 100 mM MOPS (pH 8.0), 100 μM of NADH, 100 μM acetoacetyl-CoA, 1 mM DTT (dithiothreitol), and 32 μM of *Re*PaaH1 enzyme. After pre-incubation at 30 °C for 5 min, the reaction was initiated by the addition of enzyme. The decrease in NADH was then measured at 340 nm and 30 °C using an extinction coefficient of 6.3×10^3 [28,29]. The enzyme kinetics experiments were performed by addition of various concentrations of acetoacetyl-CoA substrate, such as 10, 20, 40, 60, 80 and 100 μM.

3. Results and discussion

3.1. Overall structure of RePaaH1

To determine enzymatic properties of the *Re*PaaH1 protein, we determined the crystal structure of *Re*Paah1 at 2.6 Å. The asymmetric unit contains three *Re*PaaH1 molecules, which corresponded to one biologically active dimer and one molecule that can be generated to a dimer by crystallographic symmetry operation (Fig. 1). The size exclusion chromatography results also confirmed that *Re*PaaH1 exists as a dimer (data not shown). A search using the Dali server revealed that the structure of *Re*PaaH1 was homologous to that of human mitochondrial L-3-hydroxyacyl-CoA dehydrogenases (HuHAD) [28]. The monomeric *Re*PaaH1 structure exhibits a two-domain topology with the N- and C-terminal domains (Fig. 1C). The N-terminal domain (NTD, residues 1–188) shows a β–α–β fold similar to that in NAD^+(P)-binding proteins, and consists of a core eight-stranded β-sheet flanked by α-helices. As observed in a typical Rossmann fold, the parallel six (β1–β6) strands of the sheet run in the opposite direction to the two parallel β7 and β8 strands. A large helix-turn-helix motif (α2 and α3) connects β2 and β3, and extends from the β–α–β core. The C-terminal domain (CTD, residues 189–284) consists of five α-helices (α8–α12) and is mainly involved in dimerization

Table 1
Data collection and refinement statistics.

	SeMet	Apo	Complex with NAD$^+$	Complex with acetyl-CoA
Data collection				
Space group	$P3_221$	$P3_221$	$C2$	$C2$
Cell dimensions				
a, b, c (Å)	136.43, 136.43, 97.55	135.43, 135.43, 97.17	235.08, 135.59, 97.45	234.24, 135.37, 97.36
α, β, γ (°)	90.00, 90.00, 120.00	90.00, 90.00, 120.00	90.00, 90.09, 90.00	90.00, 90.09, 90.00
Resolution (Å)	50–2.42 (2.47–2.42)	50.0–2.6 (2.69–2.6)*	50.0–2.6 (2.69–2.60)	50.00–2.7 (2.80–2.7)
R_{sym} or R_{merge}	12.0 (44.5)	8.7 (37.4)	8.2 (34.1)	11.2 (41.0)
$I/\sigma I$	56.6 (10.2)	17.0 (2.6)	50.0 (7.1)	15.0 (6.8)
Completeness (%)	99.7	96.8 (95.4)	98.9 (99.8)	92.0 (94.0)
Redundancy	21.3 (20.4)	4.0 (3.0)	6.0 (5.5)	6.0 (6.5)
Refinement				
Resolution (Å)		50.0–2.6	50.0–2.6	50.0–2.7
No. reflections		29,327	86,885	71,952
R_{work}/R_{free}		21.4/27.1	20.2/26.9	21.3/28.5
No. atoms		6384	19,415	19,517
Protein		6306	18,918	18,918
Ligand/ion		–	396	486
Water		78	101	113
B-Factors		60.97	68.94	72.05
Protein		61.12	67.99	70.93
Ligand/ion		–	117.67	157.29
Water		49.04	55.24	52.53
R.m.s. deviations				
Bond lengths (Å)		0.011	0.012	0.011
Bond angles (°)		1.576	1.686	1.584

* Values in parentheses are for highest-resolution shell.

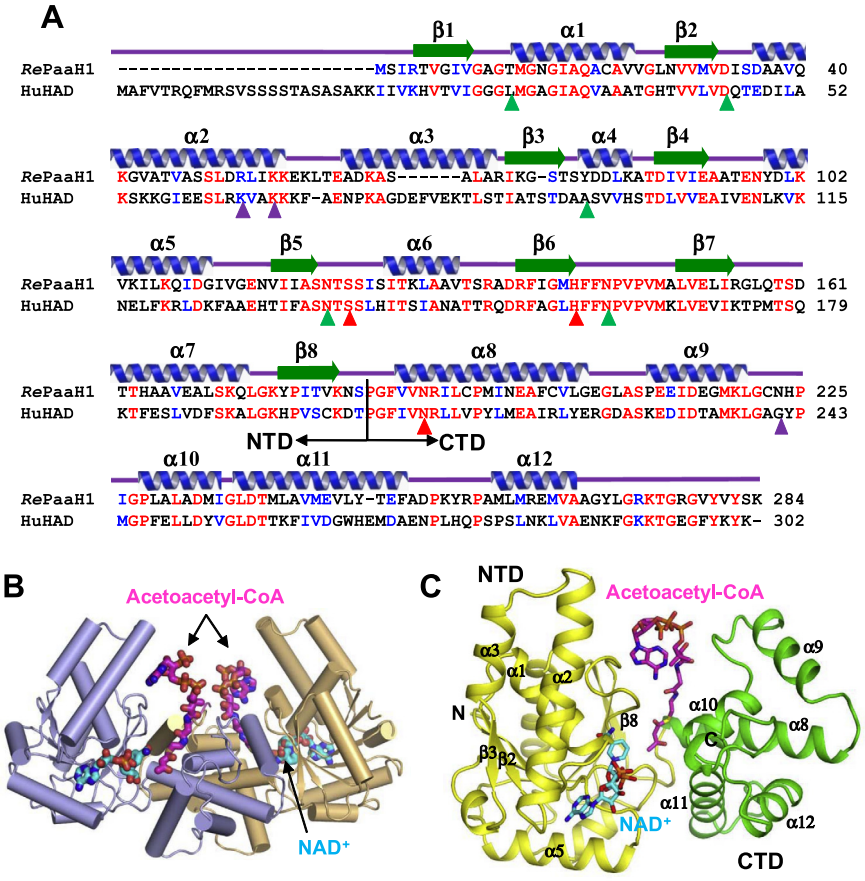

Fig. 1. Overall shape of *Re*PaaH1. (A) Amino acid sequence alignment of *Re*PaaH1 and HuHAD. Secondary structure elements are shown based on the *Re*PaaH1 structure. Identical and highly conserved residues are presented in red and blue colored characters, respectively. Residues involved in the enzyme catalysis, NAD$^+$ and substrate binding are marked with red-, green-, and purple-colored rectangles, respectively. Amino acid regions of N-terminal and C-terminal domains were indicated. (B) Overall shape of *Re*PaaH1 dimer. Two polypeptides are differentiated by colors of orange and light blue. Bound NAD$^+$ cofactor and acetoacetyl-CoA substrate were shown as stick model with cyan and magenta colors, respectively. (C) Monomeric structure of *Re*PaaH1. Monomeric structure of *Re*PaaH1 was shown as cartoon diagram, and the N-terminal domain (NTD) and the C-terminal domain (CTD) were distinguished with colors of yellow and green colors, respectively. Secondary structure elements were labeled appropriately. Bound NAD$^+$ cofactor and acetoacetyl-CoA substrate were shown as stick model with cyan and magenta colors, respectively. (For interpretation of the references to color in this figure legend, the reader is referred to the web version of this article.)

(Fig. 1C). The α8 and α9 helices of each subunit mediate dimerization through hydrophobic interactions with residues such as Val188, Val189, Ile192, Leu193, Pro195, Met196, Val203, and L208. Positively charged resides are located along the cleft between NTD and CTD, and some of these mediate the binding of the adenine diphosphate moiety of the acetoacetyl-CoA substrate, which will be described later.

3.2. RePaaH1-NAD$^+$ cofactor complex

The binding property with the NAD$^+$ cofactor was examined by determining the crystal structure of *Re*PaaH1 in complex with NAD$^+$ at a 2.6 Å resolution. The overall structure of the NAD$^+$ complex is almost identical to that of the apoenzyme, with a root-mean-square deviation of 0.25 Å on 295 Cα atoms. As expected, the NAD$^+$ cofactor is bound to the N-terminal Rossmann fold, similar to the binding seen in other structures. The NAD$^+$-binding pocket is made up of 5 loops (β1–α1, β2–α2, β4–α5, β5–α6 and β6–α7) and 1 α helix (α5) (Fig. 2A). The Thr13 and Met14 residues in the G-x-G-x-x-G nucleotide-binding motif comprised of Gly10-Ala11-Gly12-Thr13-Met14-Gly15 were paired with the two phosphate moieties of NAD$^+$ (Figs. 1A and 3A). The nicotinamide ring is recognized by the conserved residues Asn117 and Asn143, and the two ribose rings are stabilized through hydrogen bonding mediated by the side chains of the residues Asp 33 and Ser119 as well as by the main chains of the residues Ala38 and Glu92. The adenine moiety is positioned by the side chain of Tyr77 residue (Fig. 2A). The superposition of the enzyme with the NAD$^+$-bound form of HuHAD reveals that although these two enzymes share a similar NAD$^+$-binding mode, several distinct residues are observed to be involved in the NAD$^+$-binding of *Re*PaaH1. In RePaaH1, the α11 helix position is further away (by about 3 Å) from the NAD$^+$ binding site compared to the corresponding helix of HuHAD, thus rendering the nicotinamide ring binding pocket more open than that of HuHAD. The adenine moiety of NAD$^+$ is positioned at the hydrophobic cleft formed by hydrophobic residues such as Ile34, Tyr77, Ala90, Leu96 and Ile100 (Fig. 2B). However, the Tyr 77 residue also plays a role in the binding of this moiety through a hydrogen bond.

3.3. RePaaH1-acetoacetyl-CoA substrate complex

In order to examine the substrate-binding mode, we determined the crystal structure of *Re*PaaH1 in complex with the acetoacetyl-CoA substrate at a 2.5 Å resolution. The acetoacetyl-CoA substrate is positioned within the deep cleft between the NTD and CTD (Fig. 3A). The pantothenic moiety of the substrate appears

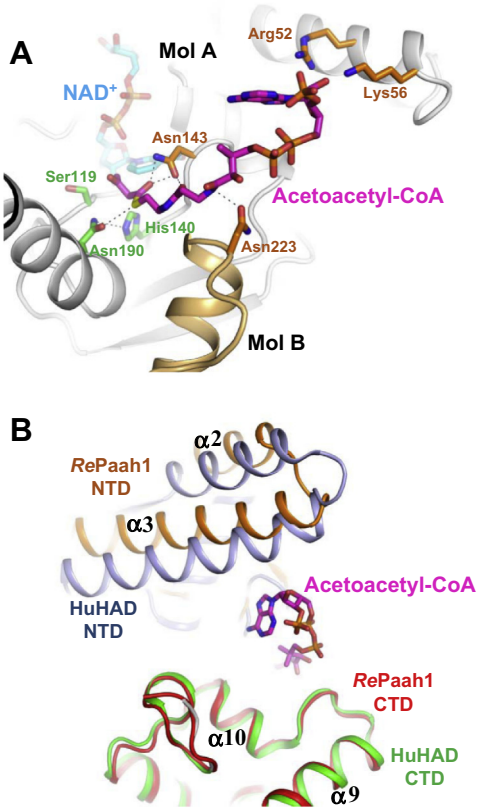

Fig. 3. Substrate-binding mode of *Re*PaaH1. (A) The *Re*PaaH1 structure was shown as a cartoon model with gray and light orange colors for each of two monomers, and labeled as Mol A and Mol B. The bound NAD$^+$ and acetoacetyl-CoA were shown as stick models with cyan and magenta colors, respectively. Residues involved in the acetoacetyl-CoA stabilization through hydrogen bonds were shown as stick models with orange color, and labeled appropriately. (B) Comparison of domain shifting between *Re*PaaH1 and HuHAD upon the substrate binding. Structures of *Re*PaaH1 and HuHAD in complex with substrate were superposed based on the C-terminal domains of the proteins. The N- and C-terminal domains of *Re*PaaH1 were shown with orange and red colors, respectively, and those of HuHAD were with light blue and green colors, respectively. The bound acetoacetyl-CoA substrate was presented as a stick model with magenta color. (For interpretation of the references to color in this figure legend, the reader is referred to the web version of this article.)

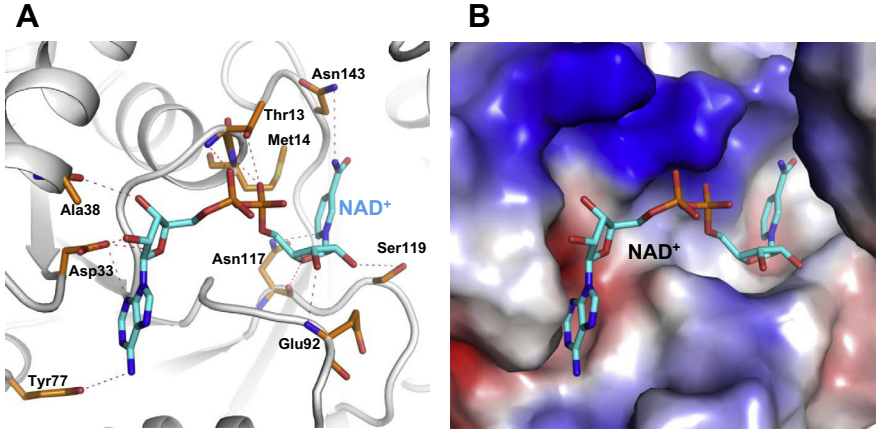

Fig. 2. NAD$^+$-binding mode of *Re*PaaH1. (A) Cartoon presentation of NAD$^+$-binding mode of *Re*PaaH1. The *Re*PaaH1 structure was shown as a cartoon model with gray color. The bound NAD$^+$ was presented as a stick model with cyan color. Residues involved in the NAD$^+$ stabilization through hydrogen bonds were shown as stick models with orange color. (B) Electrostatic potential surface presentation of NAD$^+$-binding mode of *Re*PaaH1. The *Re*PaaH1 structure was shown as an electrostatic potential surface presentation. The bound NAD$^+$ was presented as a stick model with cyan color. (For interpretation of the references to color in this figure legend, the reader is referred to the web version of this article.)

to be stabilized mainly by the side chain of Asn143 as well as the side chain of Asn223 from the other subunit of dimer through hydrogen-bond interactions. The acetoacetyl moiety is located at its binding pocket and positioned near the conserved catalytic residues Ser119, His140, and Asn190, which correspond to the Ser137, His158, and Asn208 residues of HuHAD (Fig. 3A). Interestingly, even though the two positively charged residues Arg52 and Lys56 seemed to be involved in hydrogen bonding with the adenosine moiety, the electron density map of the adenosine diphosphate moiety was not clear, indicating that the adenosine diphosphate moiety was not fully stabilized.

It is reported that a significant conformational change in the NAD^+-binding domain occurs when the domain rotates toward the C-terminal domain upon the binding of the substrate in HuHAD (Fig. 3B) [30]. However, in *Re*PaaH1, the positions of the two domains in the acetoacetyl-CoA substrate complex structure were quite similar to those of the apo-form of the protein, with a root-mean-square deviation of 0.31 Å. This result indicates that unlike HuHAD, *Re*PaaH1 does not undergo large domain shifting upon the substrate binding (Fig. 3B). Considering that *Re*PaaH1 utilizes 3-hydroxybutyryl-CoA as the main substrate while HuHAD is able to utilize 3-hydroxyacyl-CoA substrates of various lengths, we speculate that difference in the domain-shifting between these two enzymes is derived from differences in the substrate specificity.

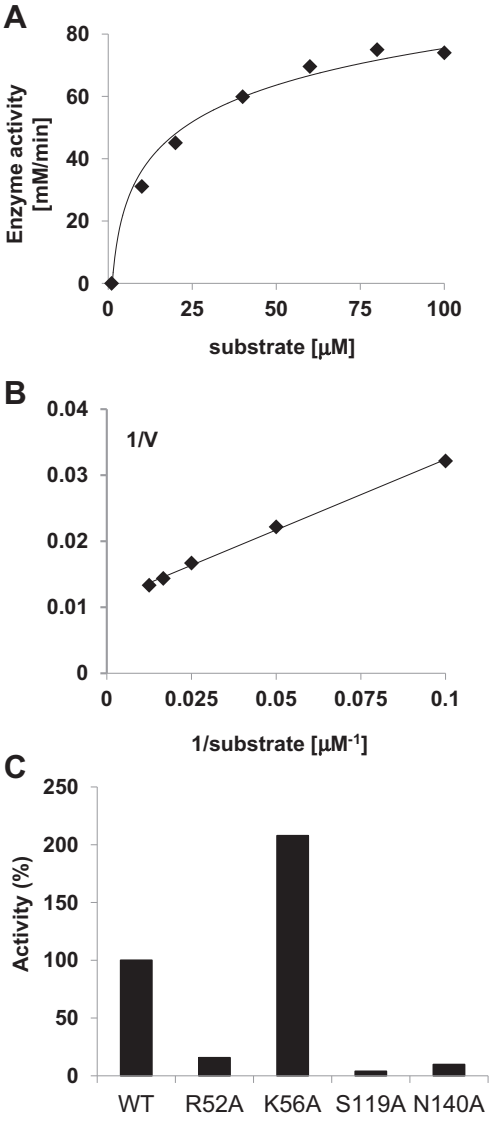

Fig. 4. Enzyme kinetics of *Re*PaaH1. (A) Michaelis–Menten equation based plot of reaction velocity versus substrate concentrations. For the various substrate concentrations, 10, 20, 40, 60, 80, and 100 mM acetoacetyl-CoA were used. (B) Lineweaver–Burk plot of (A). K_m, V_{max}, and K_{cat} of *Re*PaaH1 were calculated with 18.25 μM, 85.38 mM/min, and $4.55 \times 10^5\ s^{-1}$, respectively. (C) Site-directed mutagenesis of *Re*PaaH1. Residues involved in enzyme catalysis and substrate binding were replaced by appropriate residues. The relative activities of recombinant mutant proteins were measured and compared with that of wild-type *Re*PaaH1.

3.4. Kinetic and mutagenesis studies

To characterize the properties of *Re*PaaH1, kinetic analysis was performed by measuring the reduction in the acetoacetyl-CoA substrate levels. Reaction rates corresponding to various concentrations of acetoacetyl-CoA were plotted, and were found to obey Michaelis–Menten kinetics (Fig. 4A and B). Based on this kinetic analysis, the K_m, V_{max}, and K_{cat} values of *Re*PaaH1 with acetoacetyl-CoA were determined to be 18.25 μM, 85.38 mM/min, and $4.55 \times 10^5\ s^{-1}$, respectively.

In order to confirm the residues involved in *Re*PaaH1 catalysis and substrate binding, we performed site-directed mutagenesis experiments based on structural observations of the protein, and compared the enzymatic activity of the mutants with that of the wild-type protein. To confirm identity of the catalytic residues, two conserved residues, Ser119 and Asn190, were mutated to alanine, and the both mutants (S119A and N190A) showed almost complete loss of activity, indicating that *Re*PaaH1 uses these two residues for enzyme catalysis (Fig. 4C). As described above, the electron density of the adenosine diphosphate moiety of the acetoacetyl-CoA substrate was found to be weak, although the Arg52 and Lys56 residues are proximal to the moiety. To test if these two basic residues are involved in the binding of the adenine moiety, we generated two mutants (R52A and K56A), and compared the enzymatic activities of the mutants with that of the wild-type. Unexpectedly, the K56A mutant exhibited about a 2-fold higher activity, whereas the activity of the R52A mutant was about 15% that of the wild-type (Fig. 4C). These data indicate that the Lys56 residue does not seem to be directly involved in the binding of the adenosine moiety, and we speculate that increase in the hydrophobicity of the surface due to the alanine replacement might results in a more favorable environment for the binding of the adenosine moiety.

Acknowledgments

This work was supported by the National Research Foundation of Korea (NRF) Grant funded by the Korean Government (MEST) (NRF-2009-C1AAA001-2009-0093483) and by the Advanced Biomass R&D Center (ABC) of Global Frontier Project funded by the MEST (ABC-2012-053895), Korea.

References

[1] A. Demirbas, Political, economic and environmental impacts of biofuels: a review, Appl. Energy 86 (2009) S108–S117.
[2] O. Tirado-Acevedo, M.S. Chinn, A.M. Grunden, Production of biofuels from synthesis gas using microbial catalysts, Adv. Appl. Microbiol. 70 (70) (2010) 57–92.
[3] S.Q. Liu, N. Qureshi, How microbes tolerate ethanol and butanol, N. Biotechnol. 26 (2009) 117–121.
[4] C.R. Fischer, D. Klein-Marcuschamer, G. Stephanopoulos, Selection and optimization of microbial hosts for biofuels production, Metab. Eng. 10 (2008) 295–304.
[5] C. Xue, J.B. Zhao, L.J. Chen, F.W. Bai, S.T. Yang, J.X. Sun, Integrated butanol recovery for an advanced biofuel: current state and prospects, Appl. Microbiol. Biotechnol. 98 (2014) 3463–3474.
[6] W.J. Mitchell, Physiology of carbohydrate to solvent conversion by clostridia, Adv. Microb. Physiol. 39 (1998) 31–130.

[7] M. Inui, M. Suda, S. Kimura, K. Yasuda, H. Suzuki, H. Toda, S. Yamamoto, S. Okino, N. Suzuki, H. Yukawa, Expression of *Clostridium acetobutylicum* butanol synthetic genes in *Escherichia coli*, Appl. Microbiol. Biotechnol. 77 (2008) 1305–1316.
[8] P. Durre, Fermentative butanol production: bulk chemical and biofuel, Ann. N.Y. Acad. Sci. 1125 (2008) 353–362.
[9] P. Durre, Biobutanol: an attractive biofuel, Biotechnol. J. 2 (2007) 1525–1534.
[10] S.K. Lee, H. Chou, T.S. Ham, T.S. Lee, J.D. Keasling, Metabolic engineering of microorganisms for biofuels production: from bugs to synthetic biology to fuels, Curr. Opin. Biotechnol. 19 (2008) 556–563.
[11] Y.S. Jang, J.M. Park, S. Choi, Y.J. Choi, Y. Seung do, J.H. Cho, S.Y. Lee, Engineering of microorganisms for the production of biofuels and perspectives based on systems metabolic engineering approaches, Biotechnol. Adv. 30 (2012) 989–1000.
[12] K.T. Tran, T. Maeda, T.K. Wood, Metabolic engineering of *Escherichia coli* to enhance hydrogen production from glycerol, Appl. Microbiol. Biotechnol. 98 (2014) 4757–4770.
[13] P.I. Nikel, V. de Lorenzo, Robustness of *Pseudomonas putida* KT2440 as a host for ethanol biosynthesis, N. Biotechnol. (2014), http://dx.doi.org/10.1016/j.nbt.2014.02.006 [Epub ahead of print].
[14] K.Y. Choi, D.G. Wernick, C.A. Tat, J.C. Liao, Consolidated conversion of protein waste into biofuels and ammonia using *Bacillus subtilis*, Metab. Eng. (2014), http://dx.doi.org/10.1016/j.ymben.2014.02.007 [Epub ahead of print].
[15] M. Scheel, T. Lutke-Eversloh, New options to engineer biofuel microbes: development and application of a high-throughput screening system, Metab. Eng. 17 (2013) 51–58.
[16] T. Ezeji, C. Milne, N.D. Price, H.P. Blaschek, Achievements and perspectives to overcome the poor solvent resistance in acetone and butanol-producing microorganisms, Appl. Microbiol. Biotechnol. 85 (2010) 1697–1712.
[17] D.T. Jones, D.R. Woods, Acetone-butanol fermentation revisited, Microbiol. Rev. 50 (1986) 484–524.
[18] S. Atsumi, A.F. Cann, M.R. Connor, C.R. Shen, K.M. Smith, M.P. Brynildsen, K.J. Chou, T. Hanai, J.C. Liao, Metabolic engineering of *Escherichia coli* for 1-butanol production, Metab. Eng. 10 (2008) 305–311.
[19] D.R. Nielsen, E. Leonard, S.H. Yoon, H.C. Tseng, C. Yuan, K.L. Prather, Engineering alternative butanol production platforms in heterologous bacteria, Metab. Eng. 11 (2009) 262–273.
[20] G.W. Haywood, A.J. Anderson, L. Chu, E.A. Dawes, The role of NADH- and NADPH-linked acetoacetyl-CoA reductases in the poly-3-hydroxybutyrate synthesizing organism *Alcaligenes eutrophus*, FEMS Microbiol. Lett. 52 (1988) 259–264.
[21] H.B. Machado, Y. Dekishima, H. Luo, E.I. Lan, J.C. Liao, A selection platform for carbon chain elongation using the CoA-dependent pathway to produce linear higher alcohols, Metab. Eng. 14 (2012) 504–511.
[22] Z. Otwinowski, W. Minor, Processing of X-ray diffraction data collected in oscillation mode, Macromol. Crystallogr. 276 (Pt A) (1997) 307–326.
[23] B.W. Matthews, Solvent content of protein crystals, J. Mol. Biol. 33 (1968) 491–497.
[24] T.C. Terwilliger, J. Berendzen, Automated MAD and MIR structure solution, Acta Crystallogr. D Biol. Crystallogr. 55 (1999) 849–861.
[25] T.C. Terwilliger, Maximum-likelihood density modification, Acta Crystallogr. D Biol. Crystallogr. 56 (2000) 965–972.
[26] P. Emsley, K. Cowtan, Coot: model-building tools for molecular graphics, Acta Crystallogr. D Biol. Crystallogr. 60 (2004) 2126–2132.
[27] G.N. Murshudov, A.A. Vagin, E.J. Dodson, Refinement of macromolecular structures by the maximum-likelihood method, Acta Crystallogr. D Biol. Crystallogr. 1 (1997) 240–255.
[28] J.J. Barycki, L.K. O'Brien, J.M. Bratt, R. Zhang, R. Sanishvili, A.W. Strauss, L.J. Banaszak, Biochemical characterization and crystal structure determination of human heart short chain L-3-hydroxyacyl-CoA dehydrogenase provide insights into catalytic mechanism, Biochemistry 38 (1999) 5786–5798.
[29] R.C. Taylor, A.K. Brown, A. Singh, A. Bhatt, G.S. Besra, Characterization of a beta-hydroxybutyryl-CoA dehydrogenase from *Mycobacterium tuberculosis*, Microbiology 156 (2010) 1975–1982.
[30] J.J. Barycki, L.K. O'Brien, A.W. Strauss, L.J. Banaszak, Sequestration of the active site by interdomain shifting. Crystallographic and spectroscopic evidence for distinct conformations of L-3-hydroxyacyl-CoA dehydrogenase, J. Biol. Chem. 275 (2000) 27186–27196.